

## 7-Tesla Magnetic Resonance Imaging for Brain Iron Quantification in Homozygous and Heterozygous *PANK2* Mutation Carriers

Petr Dusek, MD, PhD,<sup>1,2,a</sup> Elena Maria Tovar Martinez, MD,<sup>3,a</sup> Vince Istvan Madai, MD,<sup>4</sup> Robert Jech, MD, PhD,<sup>1</sup> Jan Sobesky, MD,<sup>4,5</sup> Friedemann Paul, MD,<sup>6</sup> Thoralf Niendorf, PhD,<sup>3,5</sup> Jens Wuerfel, MD,<sup>2,3,5,6,b,\*</sup> Susanne A. Schneider, MD, PhD<sup>7,b,\*</sup>

**Abstract:** Pantothenate-kinase-associated neurodegeneration (PKAN) is an autosomal recessive disorder characterized by iron deposits in basal ganglia. The aim of this study was to quantify iron concentrations of deep gray matter structures in heterozygous *PANK2* mutation carriers and in PKAN patients using quantitative susceptibility mapping MRI. By determining iron concentration, we intended to find mutation-specific brain parenchymal stigmata in heterozygous *PANK2* mutation carriers in comparison to age-matched healthy volunteers. We studied 11 heterozygous *PANK2* gene mutation carriers (mean age: 43.4 years; standard deviation [SD]: 10.5), who were found to be clinically asymptomatic by neurological examination. These carriers were compared to 2 clinically affected PKAN patients 21 and 32 years of age and to 13 age-matched, healthy controls (mean age: 39.7; SD, 13.6). Scanning was performed on a 7.0-Tesla whole-body scanner applying three-dimensional susceptibility-weighted gradient echo acquisitions. Susceptibility maps were calculated by threshold-based k-space division with single-orientation acquisition. Magnetic susceptibility values, relative to the occipital white matter, were determined for the following regions of interest (ROI): globus pallidus (GP), thalamus, putamen, internal capsule (IC), caudate nucleus, substantia nigra (SN), and red nucleus. Heterozygous *PANK2* mutation carriers did not show increased brain iron concentrations, compared to healthy controls ( $P > 0.05$ ), in any of the examined ROIs. In PKAN patients, more than 3 times higher concentrations of iron were found in the GP, SN, and IC. Our results suggest that heterozygous mutations in *PANK2* gene do not cause brain iron accumulation nor do they cause movement disorders.

The syndromes of neurodegeneration with brain iron accumulation (NBIA) are defined by a progressive hypo- and/or hyperkinetic movement disorder and pathological excess of iron deposition in the brain, particularly affecting the basal ganglia, mainly the globus pallidus (GP). Of these, pantothenate-kinase-associated neurodegeneration (PKAN) is the most common form caused by mutations in the *PANK2* gene. However, PKAN is an orphan disease with an estimated world-wide prevalence of approximately 1 in 1 million.<sup>1</sup>

In NBIA syndromes, iron accumulation observed on gross pathological assessment as brown discoloration can be detected noninvasively as a prominent hypointensity in T2- and T2\*-weighted MRI.<sup>2</sup>

In PKAN, a specific MRI pattern of iron deposition, the “eye of the tiger sign” consistent with a central hyperintensity within a surrounding area of hypointensity in the anterior-medial part of the GP, is thought to be virtually pathognomonic. However, emergence of this MRI pattern appears to be a dynamic process.<sup>3,4</sup>

<sup>1</sup>Department of Neurology and Center of Clinical Neuroscience, Charles University in Prague, First Faculty of Medicine and General University Hospital in Prague, Prague, Czech Republic; <sup>2</sup>Institute of Neuroradiology, University Medicine Goettingen, Goettingen, Germany; <sup>3</sup>Berlin Ultrahigh Field Facility, Max-Delbrueck Center for Molecular Medicine, Berlin, Germany; <sup>4</sup>Department of Neurology and Center for Stroke Research Berlin, Charité-Universitaetsmedizin, Berlin, Germany; <sup>5</sup>Experimental and Clinical Research Center Charité-Universitaetsmedizin and Max Delbrueck Center for Molecular Medicine, Berlin, Germany; <sup>6</sup>NeuroCure Clinical Research Center, Charité University Medicine Berlin, Berlin, Germany; <sup>7</sup>Neurology Department, University of Kiel, Kiel, Germany

**\*Correspondence to:** Dr. Susanne A. Schneider, Department of Neurology, University of Kiel, Arnold-Heller-Straße, 24105 Kiel, Germany; E-mail: s.schneider@neurologie.uni-kiel.de or Dr. Jens Wuerfel, Institut of Neuroradiology, Universitätsmedizin Göttingen, Robert-Koch-Straße 40, 37075 Göttingen, Germany; E-mail: jens.wuerfel@charite.de

**Keywords:** pantothenate kinase associated neurodegeneration (PKAN), neurodegeneration with brain iron accumulation (NBIA), 7-Tesla MRI, quantitative susceptibility mapping, iron.

<sup>a</sup>The first two authors contributed equally.

<sup>b</sup>The last two authors contributed equally.

Relevant disclosures and conflicts of interest are listed at the end of this article.

Received 2 May 2014; revised 6 June 2014; accepted 18 June 2014.

Published online 23 October 2014 in Wiley InterScience (www.interscience.wiley.com). DOI:10.1002/mdc3.12080

It has been shown that alterations in GP detected by MRI may precede the development of clinical signs<sup>5</sup> (i.e., in asymptomatic carriers of homozygous mutations), but may also be absent in early disease stages.<sup>3,6,7</sup> Additionally, the bright spot within the surrounding area of hypointensity may vanish over time.<sup>3</sup>

Recently, a 7-Tesla (T) MRI study in 3 PKAN patients was performed using the method of field-dependent R2 relaxivity increase.<sup>8</sup> Iron concentration in GP of PKAN patients was more than doubled, compared to controls. Moreover, based on the differences in the field dependency of the relaxation rates, the researchers suggested that, in PKAN patients, iron deposited in forms other than ferritin also contributes to the MRI signal.

On the other hand, little is known about brain iron content in heterozygotes. Results of recent 3-T MRI studies suggested no signs of increased brain iron content in the 13 examined heterozygous *PANK2* mutation carriers.<sup>3</sup> However, the latter study showed subtle differences in mean water diffusivity (MD) and fractional water diffusion anisotropy (FA) in GP, cerebral peduncles, and internal capsule (IC) between heterozygous carriers and controls, which may be indirect effects reflecting altered iron content. Indeed, correlations between MD, FA, and ferritin-iron content were observed in an *in vitro* phantom study.<sup>9</sup>

Taking these results into account, the question remains of whether iron accumulation occurs in heterozygous *PANK2* mutation carriers. To answer this question, iron quantification techniques using ultra-high-field MRI can be very helpful. Changes in magnetic susceptibility of tissue resulting from iron accumulation cause magnetic field shifts on the microscopic scale. These field shifts are more closely related to iron concentration than spin-spin relaxation processes and can be detected in phase-sensitized MRIs.<sup>2</sup> Quantitative susceptibility mapping (QSM) techniques were developed to determine tissue susceptibility.<sup>10–13</sup> Ultra-high-field imaging using magnetic fields of  $B_0 \geq 7$  T is particularly sensitive to very small susceptibility changes because of the linear relationship between magnetic field strength and the field shift.<sup>14–17</sup> We used this

advantage of ultra-high-field MRI to study iron concentration in *PANK2* mutation carriers.

The aims of our study were to (1) quantify iron concentration in basal ganglia, IC, and thalami (THAs) of PKAN patients and heterozygous *PANK2* mutation carriers by employing QSM with ultra-high-field MRI and (2) seek for differences between heterozygous *PANK2* mutation carriers and healthy volunteers.

## Methods

### Participants

The study was approved by the relevant local ethic committees, and participants gave written informed consent before the study.

Two PKAN patients (both female, 21 and 32 years of age) and 11 clinically unaffected relatives of these and other PKAN patients (4 female and 7 male; mean age: 43.4 years; standard deviation [SD]: 10.5) were recruited. Patients were examined in order to determine reference susceptibility values of pronounced brain iron deposits at ultra-high field. Both patients had the atypical form of PKAN with disease onset at 12 to 14 years and duration of 7 to 20 years. Genetic testing with full sequencing of the *PANK2* gene revealed homozygous and compound heterozygous mutations, respectively, in the 2 patients and heterozygous mutations in all nonaffected family members. Thirteen age- and sex-matched healthy individuals (5 female and 8 male; mean age: 39.7 years; SD, 13.6) served as controls. All participants were neurologically examined with a focus on presence (patients) or absence (nonaffected mutation carriers and controls) of movement disorder abnormalities. Demographic and clinical characteristics are shown in Table 1.

### MRI Data Acquisition

MRIs were acquired on a Magnetom 7-T whole-body MR scanner (Siemens Healthcare, Erlangen, Germany), using a

**TABLE 1** Demographic and clinical characteristics of patients and heterozygous mutation carriers

Proband	Nationality	Age	Clinical Status (Age at Onset)	Disease Severity (BFM Score)	Genetic Status
PKAN-1	Czech	21	Generalized dystonia, spasticity (R>L), micrographia, dysarthria, dysphagia, drooling, personality changes (14 years)	27	c.1253C>T (homozygous)
PKAN-2	Czech	32	Generalized dystonia, Babinski sign positive (R>L), gait freezing, dysarthria, dysphagia, drooling, personality changes (12 years)	62	c.1369G>T and c.1561G>A
Non-Manif-1	Polish	43	Unaffected	n/a	c.573delC
Non-Manif-2	Polish	41	Unaffected	n/a	c.1583C>T
Non-Manif-3	Czech	29	Unaffected	n/a	c.1253C>T
Non-Manif-4	Czech	26	Unaffected	n/a	c.1253C>T
Non-Manif-5	Czech	56	Unaffected	n/a	c.1253C>T
Non-Manif-6	Czech	47	Unaffected	n/a	c.1253C>T
Non-Manif-7	Argentinian	47	Unaffected	n/a	c.821-822del
Non-Manif-8	Czech	54	Unaffected	n/a	c.1369G>T
Non-Manif-9	Czech	56	Unaffected	n/a	c.1561G>A
Non-Manif-10	German	40	Unaffected	n/a	Deletion exon 5
Non-Manif-11	German	39	Unaffected	n/a	c.1663-1G>C

BFM, Burke Fahn Marsden Dystonia Rating Scale; Non-Manif, nonmanifesting heterozygous gene mutation carrier; n/a, not applicable.

24-channel receive head coil (Nova Medical, Wilmington, MA). The subject's head was carefully padded with foam cushions during the entire measurement to avoid head movements. A three-dimensional (3D) flow-compensated susceptibility-weighted imaging (SWI) gradient echo technique was employed (echo time [TE] = 15 ms; repetition time [TR] = 25 ms; flip angle = 12 degrees; 72 slices; matrix = 448 × 352; spatial resolution: 0.5 × 0.5 × 1.0 mm<sup>3</sup>). In PKAN patients, turbo inversion recovery magnitude (TIRM; TE = 90 ms; TR = 10,070 ms; inversion time [TI] = 2,614 ms; flip angle = 128 degrees; 35 slices; matrix = 512 × 448; spatial resolution: 0.5 × 0.5 × 3.0 mm<sup>3</sup>) and 3D magnetization-prepared rapid acquisition with gradient echo (MP-RAGE; TE = 2.98 ms; TR = 2,300 ms; TI = 900 ms; flip angle = 5 degrees; matrix = 256 × 240; spatial resolution: 1.0 × 1.0 × 1.0 mm<sup>3</sup>) techniques were also employed.

### Data Processing and Susceptibility Calculation

For the calculation of the susceptibility maps, the phase images derived from the high-resolution SWI data sets were high-pass filtered and divided into the original complex image to remove effects of large-scale background magnetic fields (e.g., air-tissue boundaries at the sinuses). This processing yields a homodyne high-pass-filtered phase image, with most low spatial frequency phases removed.<sup>18</sup>

To keep the field of view with an aspect ratio of 1:1:4, k-space was interpolated by zero filling the phase images to a 512 × 512 × 128 three-dimensional matrix. Susceptibility calculations using a regularized inverse filter were performed in the selected 3D regions of the Fourier transform of the high-pass-filtered phase image (Fig. 1).<sup>19</sup>

### Image and Region of Interest Analysis

Seven regions of interest (ROIs) were placed into the deep gray matter structures bilaterally to evaluate the dependence of the calculated susceptibility values in the iron-rich deep gray matter structures on the iron content, namely, the GP, THA, putamen (PUT), caudate nucleus (CN), substantia nigra (SN), and red nucleus (RN). An additional ROI was placed into the IC. ROIs were manually plotted on the susceptibility maps.

We calculated the difference in susceptibility values of each structure relative to the occipital white matter; values of both hemispheres were averaged. The occipital white matter was used as a reference, considering that this region exhibits the lowest intersubject variance in iron concentration and shows no iron deposits in pathological states.<sup>20</sup>

### Statistical Analysis

Statistical analyses were conducted using GraphPad Prism software (GraphPad Software Inc., San Diego, CA). A normality test was performed using Kolmogorov-Smirnov's test, and the phase and susceptibility data showed a normal distribution.

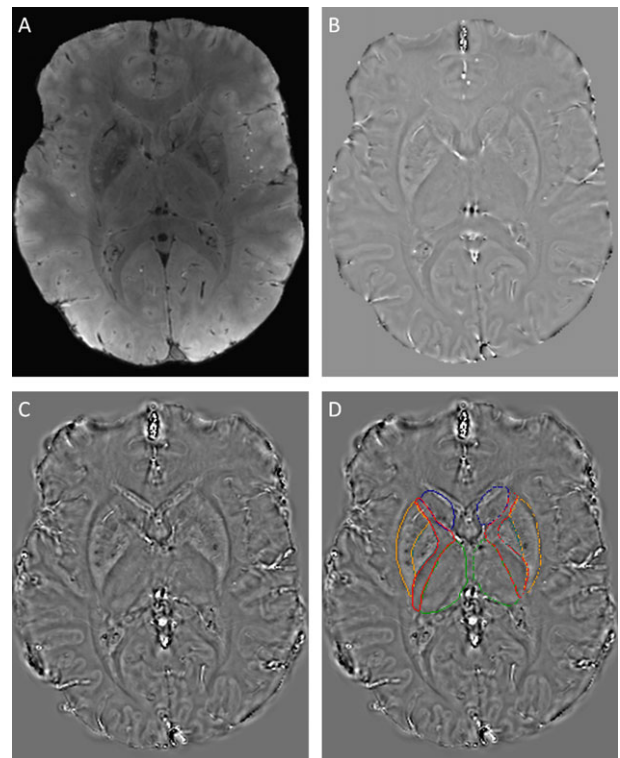


**Figure 1** Output of image-processing steps. (A) Magnitude image, (B) unwrapped filtered phase image, (C) susceptibility map calculated by thresholded k-space division with single-orientation acquisition, and (D) susceptibility map with ROIs highlighted in color: blue, caudate nucleus; orange, putamen; dark green, globus pallidus; red, internal capsule; green, thalamus.

Two-tailed *t* tests with false discovery rate correction were performed to compare ROI susceptibility values of relatives and healthy controls. To calculate iron content, the following steps were performed: In healthy volunteers, the mean susceptibility values in every ROI were plotted against the iron content of each corresponding region, as reported by Hallgren and Sourander, in a postmortem analysis.<sup>21</sup> Pearson's correlation coefficient and linear regression fit were calculated. Using the linear regression fit, iron content was then calculated based on measured susceptibility values for all study participants.

### Results

In healthy volunteers, a strong positive linear correlation between regional bulk magnetic susceptibility and reported postmortem iron concentration<sup>21</sup> was found (Fig. 2A). Including all ROIs, the linear regression fit yielded:  $\chi = 0.57 \text{ ppb} \times [\text{Fe}] + 43.625$ , where [Fe] is the iron concentration in  $\mu\text{g/g}$  wet tissue mass and the susceptibility value  $\chi$  is referenced to the mean susceptibility of occipital white matter ( $r^2 = 0.9321$ ). The results of the regional QSM analysis to calculate iron content using the linear regression fit are summarized in Table 2.

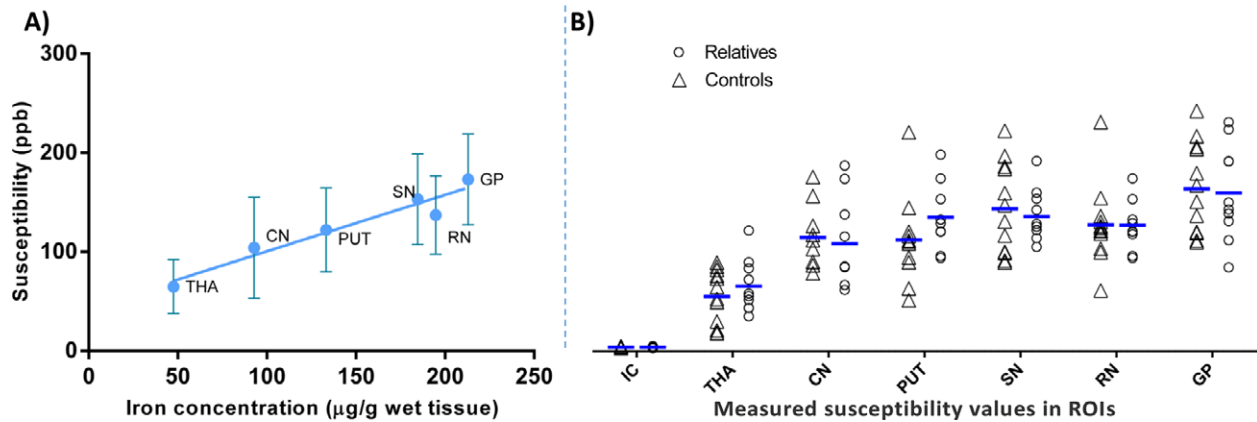


**Figure 2** (A) Average susceptibility values in healthy controls plotted against estimated nonheme iron content based on the work of Hallgren and Sourander<sup>21</sup> for the following brain regions (iron concentration values presented as mean  $\pm$  SD  $\mu\text{g/g}$ ): TH (47.6  $\pm$  1); CN (92.8  $\pm$  2); PUT (133.2  $\pm$  3); SN (184.6  $\pm$  7); RN (194.8  $\pm$  7); and GP (213.0  $\pm$  3). The calculated slope of the linear regression fit 0.57  $\pm$  0.1 ppb per  $\mu\text{g}$  iron per g of wet tissue, which is in good agreement with the values of 0.56 and 0.6 previously reported by Shmueli et al.<sup>31</sup> and Wharton and Bowtell<sup>32</sup>, respectively. (B) Differences in the magnetic susceptibility of the ROIs, relative to the occipital white matter, for all subjects in both study groups. Heterozygotes showed no significant increased magnetic susceptibility versus the healthy controls ( $P > 0.05$ ) in any of the ROIs. Y-axis scale is equal for part (A) and (B).

**TABLE 2** Mean bulk tissue magnetic susceptibilities (in ppb) and the corresponding iron concentrations ( $\mu\text{g/g}$  wet tissue) in healthy volunteers, heterozygous relatives, and patients

ROI	Controls		Relatives		Patient 1		Patient 2	
	Bulk Susceptibility (ppb)	Iron Concentration ( $\mu\text{g/g}$ wet tissue)	Bulk Susceptibility (ppb)	Iron Concentration ( $\mu\text{g/g}$ wet tissue)	Bulk Susceptibility (ppb)	Iron Concentration ( $\mu\text{g/g}$ wet tissue)	Bulk Susceptibility (ppb)	Iron Concentration ( $\mu\text{g/g}$ wet tissue)
GP	173 $\pm$ 45	228	169 $\pm$ 47	220	605	986	465	740
RN	137 $\pm$ 39	164	136 $\pm$ 40	162	156	198	142	173
SN	153 $\pm$ 46	193	145 $\pm$ 45	178	628	1026	593	965
PUT	122 $\pm$ 42	138	144 $\pm$ 32	176	135	161	138	166
CN	104 $\pm$ 51	107	98 $\pm$ 55	96	110	117	106	110
THA	65 $\pm$ 27	37	75 $\pm$ 26	55	56	21	73	52
IC	4 $\pm$ 2	N.D.	4 $\pm$ 2	N.D.	19	N.D.	22	N.D.

Susceptibility values are given relative to the occipital white matter region. Iron concentration was not calculated for IC because the relationship between susceptibility and iron concentration is not linear in white matter and cannot be reliably derived from the linear regression equation calibrated on deep gray matter structures. N.D., not done.

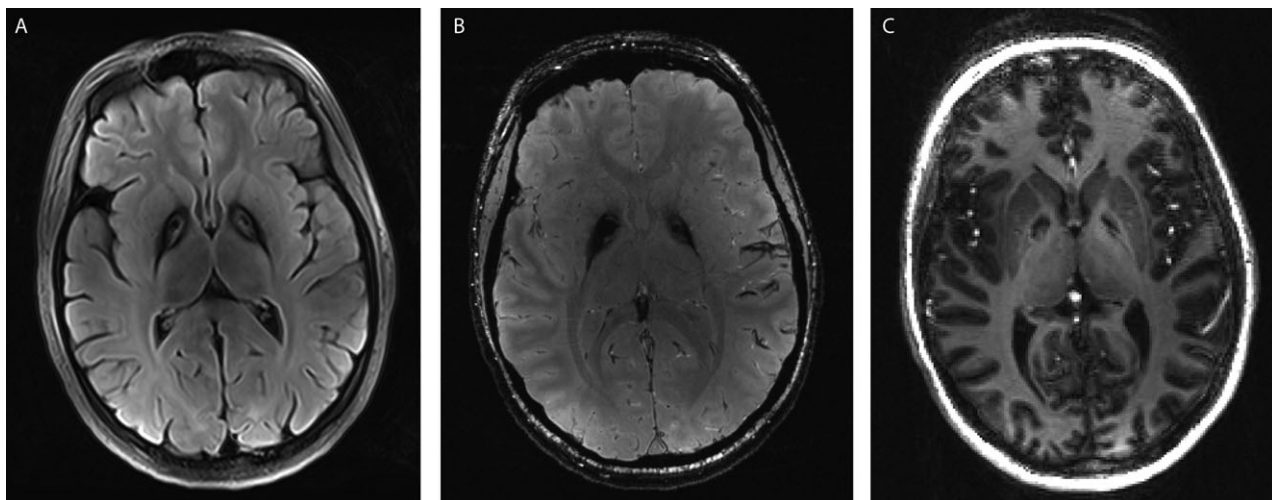


**Figure 3** PKAN patient: the eye of the tiger sign, that is, hypointense signal in the GP with a central region of hyperintensity clearly visible in the TIRM image (A) that is barely apparent on the SWI image (B). MP-RAGE image shows only hypointense signal in the antero-medial part of the GP (C).

Figure 2B shows the mean susceptibility values in each ROI for healthy controls and *PANK2* mutation carriers. *PANK2* mutation heterozygotes did not exhibit significantly increased concentration of iron, compared to healthy controls ( $P > 0.05$ ), in any ROI nor did they exhibit any signs of movement disorders in neurological examination.

We found the typical eye of the tiger sign in patients showing iron-deposits-related hypointensity in T2-weighted (T2w) MRIs with a central T2w hyperintensity, presumably representing gliotic changes and edema, as indicated by the magnitude images derived from TIRM and SWI imaging (Fig. 3). In PKAN patients, considerably higher susceptibility values were found in the GP, SN, and IC (Table 2). In the GP of the 2 PKAN patients, susceptibility values were 465 to 605 parts per billion (ppb), in comparison to the mean value  $173 \pm$  (SD) 45 ppb in healthy controls. In the SN, the 2 patients had 4 times higher susceptibility values (593–628 ppb), compared to healthy controls ( $153 \pm 46$  ppb); in the IC, susceptibility values were 5 times increased in patients (19–22 ppb; healthy controls:  $4 \pm 2$  ppb). No differences in iron concentrations were detected in other ROIs (THA, PUT, CN, and RN). When the calculated iron concentrations in GP for *PANK2* mutation heterozygotes and healthy controls were plotted against age, we did not reveal differences in the slope of age-related iron content changes between these groups (data not shown).

## Discussion

We employed QSM using 7-T MRI to characterize and quantify the iron distribution in the basal ganglia of PKAN patients and asymptomatic heterozygous *PANK2* gene mutation carriers and compared these to age-matched healthy controls. QSM was used to make sure that the susceptibility weighting would be dictated by microscopic  $B_0$  susceptibility gradients, rather than by macroscopic  $B_0$  field inhomogeneities. For this purpose, a threshold k-space division with single-orientation acquisition was employed. Our iron concentration estimates derived from susceptibility values are highly correlated with postmortem iron concentration values,<sup>21</sup> confirming the validity of this approach.

The major aim of this study was to ascertain whether asymptomatic relatives with heterozygous gene mutations show subtle signs of iron accumulation that could be used as an endophenotypic marker, similar to mild abnormalities observed in heterozygous gene mutation carriers of other recessive movement disorders, such as Parkin-related parkinsonism.<sup>22,23</sup> However, we did not detect signs of abnormal iron deposits in healthy heterozygotes with high spatial resolution 7-T MRI. This finding argues against abnormalities in brain iron metabolism in subjects carrying a single abnormal *PANK2* allele. Consequently, our results do not support the idea that subtle changes in FA and MD in heterozygous gene carriers detected by Delgado et al. are reflections of iron deposits.

The group of examined heterozygotes covers the age spectrum of the third to sixth decade, and the slope of age-related iron accumulation in GP in this age group was not significantly

different, compared to healthy controls. However, because we did not examine heterozygous subjects in the seventh decade or older, we cannot confidently exclude that abnormal iron accumulation occurs in this age group. It is also important to note that the *PANK2* enzyme is not involved in iron metabolism, but in coenzyme A synthesis. Thus, iron accumulation may be only a secondary factor in the pathophysiology of PKAN and may not be best suited as an endophenotypic marker of heterozygous *PANK2* mutation. Instead, heterozygotes may manifest other subtle metabolic abnormalities (e.g., in lipid or energy metabolism).<sup>24</sup> Absence of movement disorders in examined heterozygotes suggests, however, that any abnormality, if potentially present, would not be clinically significant.

It was suggested that, besides ferritin, part of the iron deposits in PKAN patients is composed of a ferromagnetic compound with similar properties as superparamagnetic iron oxide nanoparticles.<sup>8</sup> Our approach does not distinguish between these iron forms. Nevertheless, the QSM method is capable of detecting iron in any form with magnetic properties. Thus, even if superparamagnetic iron accumulation occurred in heterozygous gene carriers, it would have been detected by our approach.

As expected, we detected a significant increase of iron in the GP of our patients of more than 3 times, compared to controls. The iron concentration in GP measured by QSM (mean, 863  $\mu\text{g/g}$ ) was higher than previous results obtained by R2 relaxivity measurements (mean, 443 and 480  $\mu\text{g/g}$ , respectively).<sup>8,25</sup> Because we scanned only 2 PKAN patients, our sample is not representative, and no solid conclusion can be drawn regarding over- or underestimation of the iron concentration while using the QSM or R2 relaxivity approach, respectively. Notably, no MRI method is sufficiently validated for measurement of brain iron concentration in pathological states with profound iron deposits, and calculated values should be thus treated as rough estimates.

The eye of the tiger sign was best appreciated using the TIRM sequence, whereas in the SWI sequence, the sign was not as clearly visible as a result of the strong T2w signal extinction resulting from the deposited iron (Fig. 3). The presence of the eye of the tiger sign thus strongly depends on the MRI parameters used.

In line with recent literature,<sup>3,26,27</sup> iron deposition extended to adjacent areas in our patients, namely, to the SN and IC, which was reflected in clinical symptoms of mild parkinsonism and pyramidal signs in addition to generalized dystonia. Indeed, dopamine transporter single-photon emission CT, as a marker of dopamine loss in Parkinson's disease, may be abnormal in PKAN.<sup>28</sup> Similarly, GP and SN signal abnormalities in PKAN patients were reported for diffusion tensor imaging,<sup>3,29</sup> presenting with pseudoincreased FA and abnormal MD. These abnormalities are, however, likely to be consequences of iron deposits disturbing the local magnetic field.<sup>9</sup> Transcranial ultrasound investigations<sup>30</sup> also support the involvement of GP and SN, showing hyperechogenicity of the SN and nucleus lentiformis hypothesized to represent the correlate of iron deposits.

In conclusion, we did neither observe signs of movement disorders nor increased iron accumulation in heterozygous carri-

ers of *PANK2* gene mutation. This implies that a single functional *PANK2* allele is sufficient for normal function.

## Author Roles

(1) Research Project: A. Conception, B. Organization, C. Execution; (2) Statistical Analysis: A. Design, B. Execution, C. Review and Critique; (3) Manuscript: A. Writing of the First Draft, B. Review and Critique.

P.D.: 1A, 1B, 1C, 3A, 3B

E.M.T.M.: 1A, 1B, 1C, 2B, 3B

V.I.M.: 1A, 1B, 1C, 3B

R.J.: 1A, 1B, 1C, 3B

J.S.: 1A, 1B, 1C, 3B

F.P.: 1A, 1B, 1C, 3B

T.N.: 1A, 1B, 1C, 3B

J.W.: 1A, 1B, 1C, 3B

S.A.S.: 1A, 1B, 1C, 3A, 3B

## Acknowledgments

The authors thank the patients and their relatives, as well as the healthy controls, for participating in our study and Hoffnungsbaum e.V. for their support.

## Disclosures

**Funding Sources and Conflicts of Interest:** Petr Dusek received funding from the Charles University in Prague with the grant PRVOUK-P26/LF1/4. Vince Madai and Jan Sobesky received funding from the German Federal Ministry of Education and Research with the grant “Center for Stroke Research Berlin” (01 EO 0801; <http://www.bmbf.de>). Robert Jech received funding from the Czech Ministry of Health with the grant IGA MZ ČR NT12282-5/2011 and from the Charles University in Prague with the grant PRVOUK-P26/LF1/4. Friedemann Paul is supported by the German Research Foundation (Exc 257). Thoralf Niendorf has nothing to disclose related to the project. Susanne A. Schneider received funding from Else Kroener-Fresenius-Stiftung, Eva Luise und Horst Köhler-Stiftung, and the Novartis Pharma GmbH.

**Financial Disclosures for previous 12 months:** The study was supported by the Else Kröner-Fresenius-Stiftung, the Eva Luise und Horst Köhler Stiftung, the Novartis Pharma GmbH, the German Federal Ministry of Education and Research, and by the Czech Ministry of Education (research project PRVOUKP26/LF1/4). None of the funding bodies had any input into the study design or analysis.

## References

- Kruer MC, Boddaert N, Schneider SA, et al. Neuroimaging features of neurodegeneration with brain iron accumulation. *AJNR Am J Neuroradiol* 2012;33:407–414.
- Haacke EM, Cheng NY, House MJ, et al. Imaging iron stores in the brain using magnetic resonance imaging. *Magn Reson Imaging* 2005;23:1–25.
- Delgado RF, Sanchez PR, Speckter H, et al. Missense *PANK2* mutation without “eye of the tiger” sign: MR findings in a large group of patients with pantothenate kinase-associated neurodegeneration (PKAN). *J Magn Reson Imaging* 2012;35:788–794.
- Hayflick SJ, Hartman M, Coryell J, Gitschier J, Rowley H. Brain MRI in neurodegeneration with brain iron accumulation with and without *PANK2* mutations. *AJNR Am J Neuroradiol* 2006;27:1230–1233.
- Hayflick SJ, Penzien JM, Michl W, Sharif UM, Rosman NP, Wheeler PG. Cranial MRI changes may precede symptoms in Hallervorden-Spatz syndrome. *Pediatr Neurol* 2001;25:166–169.
- Chiapparini L, Savoirdo M, D’Arrigo S, et al. The “eye-of-the-tiger” sign may be absent in the early stages of classic pantothenate kinase associated neurodegeneration. *Neuropediatrics* 2011;42:159–162.
- Aggarwal A, Schneider SA, Houlden H, et al. Indian-subcontinent NBIA: unusual phenotypes, novel *PANK2* mutations, and undetermined genetic forms. *Mov Disord* 2010;25:1424–1431.
- Dezortova M, Herynek V, Krssak M, Kronerwetter C, Trattnig S, Hajek M. Two forms of iron as an intrinsic contrast agent in the basal ganglia of PKAN patients. *Contrast Media Mol Imaging* 2012;7:509–515.
- Rulseh AM, Keller J, Tintera J, Kozisek M, Vymazal J. Chasing shadows: what determines DTI metrics in gray matter regions? An in vitro and in vivo study. *J Magn Reson Imaging* 2013;38:1103–1110.
- Liu J, Liu T, de Rochefort L, et al. Morphology enabled dipole inversion for quantitative susceptibility mapping using structural consistency between the magnitude image and the susceptibility map. *Neuroimage* 2012;59:2560–2568.
- Marques JP, Bowtell R. Application of a Fourier-based method for rapid calculation of field inhomogeneity due to spatial variation of magnetic susceptibility. *Concepts Magn Reson Part B Magn Reson Eng* 2005;25B:65–78.
- Salomir R, de Senneville BD, Moonen CTW. A fast calculation method for magnetic field inhomogeneity due to an arbitrary distribution of bulk susceptibility. *Concepts Magn Reson* 2003;19B:26–34.
- Schweser F, Deistung A, Lehr BW, Reichenbach JR. Quantitative imaging of intrinsic magnetic tissue properties using MRI signal phase: an approach to in vivo brain iron metabolism? *Neuroimage* 2011;54:2789–2807.
- de Rochefort L, Liu T, Kressler B, et al. Quantitative susceptibility map reconstruction from MR phase data using Bayesian regularization: validation and application to brain imaging. *Magn Reson Med* 2010;63:194–206.
- Wharton S, Schafer A, Bowtell R. Susceptibility mapping in the human brain using threshold-based k-space division. *Magn Reson Med* 2010;63:1292–1304.
- Turner R, Jezzard P, Wen H, et al. Functional mapping of the human visual cortex at 4 and 1.5 Tesla using deoxygenation contrast EPI. *Magn Reson Med* 1993;29:277–279.
- Meloni A, Hezel F, Positano V, et al. Detailing magnetic field strength dependence and segmental artifact distribution of myocardial effective transverse relaxation rate at 1.5, 3.0, and 7.0 T. *Magn Reson Med* 2014;71:2224–2230.
- Haacke EM, Xu Y, Cheng YC, Reichenbach JR. Susceptibility weighted imaging (SWI). *Magn Reson Med* 2004;52:612–618.
- Haacke EM, Tang J, Neelavalli J, Cheng YC. Susceptibility mapping as a means to visualize veins and quantify oxygen saturation. *J Magn Reson Imaging* 2010;32:663–676.
- Langkammer C, Schweser F, Krebs N, et al. Quantitative susceptibility mapping (QSM) as a means to measure brain iron? A post mortem validation study. *Neuroimage* 2012;62:1593–1599.
- Hallgren B, Sourander P. The effect of age on the non-haemin iron in the human brain. *J Neurochem* 1958;3:41–51.
- Binkofski F, Reetz K, Gaser C, et al. Morphometric fingerprint of asymptomatic Parkin and *PINK1* mutation carriers in the basal ganglia. *Neurology* 2007;69:842–850.
- Schneider SA, Talelli P, Cheeran BJ, et al. Motor cortical physiology in patients and asymptomatic carriers of parkin gene mutations. *Mov Disord* 2008;23:1812–1819.
- Leoni V, Strittmatter L, Zorzi G, et al. Metabolic consequences of mitochondrial coenzyme A deficiency in patients with *PANK2* mutations. *Mol Genet Metab* 2012;105:463–471.

25. Hajek M, Adamovicova M, Herynek V, et al. MR relaxometry and 1H MR spectroscopy for the determination of iron and metabolite concentrations in PKAN patients. *Eur Radiol* 2005;15:1060–1068.
26. Fermin-Delgado R, Roa-Sanchez P, Speckter H, et al. Involvement of globus pallidus and midbrain nuclei in pantothenate kinase-associated neurodegeneration: measurement of T2 and T2\* time. *Clin Neuroradiol* 2013;23:11–15.
27. Kruer MC, Hiken M, Gregory A, et al. Novel histopathologic findings in molecularly-confirmed pantothenate kinase-associated neurodegeneration. *Brain* 2011;134(Pt 4):947–958.
28. Antonini A, Goldwurm S, Benti R, et al. Genetic, clinical, and imaging characterization of one patient with late-onset, slowly progressive, pantothenate kinase-associated neurodegeneration. *Mov Disord* 2006;21:417–418.
29. Awasthi R, Gupta RK, Trivedi R, Singh JK, Paliwal VK, Rathore RK. Diffusion tensor MR imaging in children with pantothenate kinase-associated neurodegeneration with brain iron accumulation and their siblings. *AJNR Am J Neuroradiol* 2010;31:442–447.
30. Kostic VS, Svetel M, Mijajlovic M, Pavlovic A, Jecmenica-Lukic M, Kozic D. Transcranial sonography in pantothenate kinase-associated neurodegeneration. *J Neurol* 2012;259:959–964.
31. Shmueli K, de Zwart JA, van Gelderen P, Li TQ, Dodd SJ, Duyn JH. Magnetic susceptibility mapping of brain tissue in vivo using MRI phase data. *Magn Reson Med* 2009;62:1510–1522.
32. Wharton S, Bowtell R. Whole-brain susceptibility mapping at high field: a comparison of multiple- and single-orientation methods. *Neuroimage* 2010;53:515–525.